NANO LETTERS
Cite This: Nano Lett. 2019, 19, 629–634
Letter
pubs.acs.org/NanoLett

Silicon Nanoribbon pH Sensors Protected by a Barrier Membrane with Carbon Nanotube Porins

Xi Chen,[†,‡] Huanan Zhang,[†,§] Ramya H. Tunuguntla,[†,∥] and Aleksandr Noy*[,†,‡]

[†]Physical and Life Sciences Directorate, Lawrence Livermore National Laboratory, Livermore, California 94550, United States
[‡]School of Natural Sciences, University of California Merced, Merced, California 95343, United States

ABSTRACT: Limited biocompatibility and fouling propensity can restrict real-world applications of a large variety of biosensors. Biological systems are adept at protecting and separating vital components of biological machinery with semipermeable membranes that often contain defined pores and gates to restrict transmembrane transport only to specific species. Here we use a similar approach for creating fouling-resistant pH sensors. We integrate silicon nanoribbon transistor sensors with an antifouling lipid bilayer coating that contains proton-permeable carbon nanotube porin (CNTP) channels and demonstrate robust pH detection in a variety of complex biological fluids.

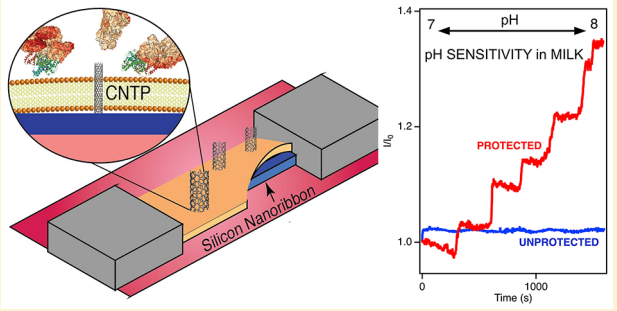

KEYWORDS: *Carbon nanotube porins, silicon nanoribbon sensors, biosensing, antifouling coating*

Biological signaling mechanisms often involve small molecules, ions,[1] and protons and facile in situ monitoring of the levels of these species is vital for medical diagnostics. Even the simplest signals, such as intracellular pH level can provide important information: for example, acidification of tumors because of elevated glucose uptake and lactic acid release is a biomarker of cancer cells.[2] Acidification of extracellular fluid is also one of the key processes during epileptic seizures, and monitoring and controlling pH of extracellular fluid has diagnostic and therapeutic potential.[3] Of all biosensing platforms, electrical sensors represent the best opportunity to develop implantable long-term sensing platforms because of their typically high sensitivity levels, fast response, and ease of multiplexing, signal processing, and coupling to wireless readout components.[4,5]

Although ion-selective electrodes represent the most ubiquitous electrical ion sensing platform, field effect transistors (FETs) have matured into a versatile alternative sensing platform that excels at continuous monitoring of small analyte levels.[6] FET sensors typically respond to the changes in the surface potential on the device channel region due to analyte binding or local ionization events and then amplify this signal using the high intrinsic transistor gain. Silicon nanowire/nanoribbon devices that exploited tailorable nature of silicon, advances in nanowire synthesis, and the existing mature silicon processing technologies have developed into a versatile platform for real-time, label-free, highly sensitive detection of disease biomarkers,[7−12] DNA mismatches,[13−15] and viruses.[16]

As the FET-based biosensing and diagnostic platforms move into the realms of clinical use and potentially even long-term implantable applications, some of the limitations of the technology come into sharp relief, especially those related to device fouling in complex fluid environments. Researchers have used different fouling mitigation strategies based on polymeric surface coatings,[17−19] bioinspired functionalization approaches,[20,21] and low-adhesion coatings.[22] Another general strategy to mitigate fouling is based on separating the sensing surface, which houses the analyte targets, from the measuring surface of the FET device. To implement this strategy, researchers developed sensors with side gate,[23] floating gate,[24,25] and dual gate.[26,27] We have also proposed an alternative strategy that uses a semipermeable lipid membrane coating on a device that incorporates specific membrane channels that isolates the sensor surface from the solution and only allows the species of interest to reach the device sensing surface.[28,29] In the past, we have demonstrated the versatility of this approach by creating SiNW FET devices that incorporate specific ion channels,[29] and ion pumps.[30]

To create robust pH FET sensors based on this principle, the lipid membrane needs to incorporate a robust channel that is highly permeable (and, ideally, highly specific) to protons. We have recently demonstrated that narrow 0.8 nm diameter carbon nanotube porins (CNTPs),[31,32] about 10 nm carbon nanotube (CNT) segments that spontaneously insert into a lipid membrane and form transmembrane channels, have extremely high proton permeability that is an order of magnitude higher than proton permeability of bulk water. Inert smooth surface of the 0.8 nm diameter nanotube pores, which is responsible for creating conditions that favor fast proton transport, also ensures that CNTPs can effectively

Received: July 16, 2018
Revised: September 20, 2018
Published: October 4, 2018

DOI: 10.1021/acs.nanolett.8b02898
Nano Lett. 2019, 19, 629–634

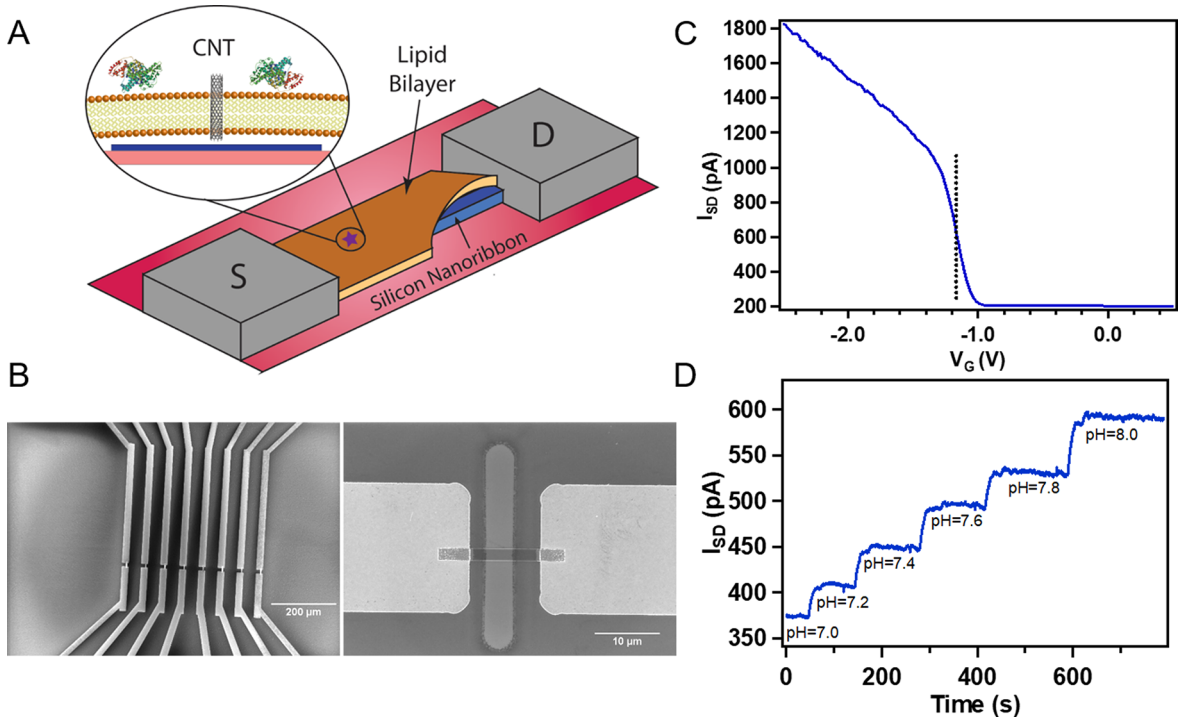

Figure 1. Silicon nanoribbon (SiNR) field-effect transistors. (A) Schematics showing a silicon nanoribbon transistor device coated with the protective lipid layer. Source and drain electrodes of the device are marked as S and D, respectively. Inset shows a magnified region of the device showing carbon nanotube porins inserted into the lipid bilayer. (B) Scanning electron microscopy images of (left) an area of the chip showing several devices, and (right) a magnified image of an individual transistor device showing the source and drain electrodes connected with a nanoribbon and channel etched in the passivating layer to expose the central part of the ribbon. (C) A plot of the source-drain current, I_{SD}, versus gate voltage, V_G (transfer characteristics), for an uncoated SiNR device. Dashed line indicates the gate voltage of −1.18 V, corresponding to the maximum transconductance of 3.8 nS. (D) Time trace of the source-drain current (I_{SD}) of the uncoated device recorded as it was exposed to different pH buffer solutions (pH values indicated on the graph).

block most of the fouling components of biological mixtures and prevent them from reaching the sensor surface.

In this work, we integrate the lipid membrane with small diameter CNTP pores with silicon nanoribbon (SiNR) field-effect transistor pH sensors. We show that this lipid−CNTP barrier membrane does not degrade the sensing performance of SiNR FET devices. Moreover, long-term fouling tests show that the lipid−CNTP coating makes SiNR FET sensors quite resistant to fouling by a range of complex biological fluids.

Majority of silicon nanowire FET devices described in the literature fall into two loosely defined categories of "bottom-up" fabricated devices that use silicon nanowires fabricated by catalytic CVD and subsequently transferred onto the device wafer[33,34] and "top-down" fabricated devices in which silicon nanowires or nanoribbons (SiNRs) are etched from a thin top layer of silicon-on-insulator (SOI) wafer.[11] For this work, we have used the second approach because it allowed us to fabricate a large number of devices with identical geometry on the wafer, although we note that our approach would be equally applicable to the "bottom-up" fabricated family of devices.

We used the "top-down" approach to fabricate FET devices with 2 μm wide SiNR channels (Figure 1B). The device sensitivity and signal-to-noise ratio (SNR) can be optimized by tuning the geometrical dimensions of the device. In this work, we primarily focus on micron-scale nanoribbons, which simplify the fabrication process. The relatively wide channel surface characteristic of this device architecture also simplifies lipid membrane fusion on the SiNR and ensures that the coated surface would contain a large number of CNTPs. We also coated the SiNRs with a thin (10 nm) layer of SiO_2 deposited by atomic layer deposition, which after rapid thermal annealing step created a pinhole-free dielectric layer on the SiNR. Nanoribbons were then connected to nickel source and drain electrodes with nickel silicide contacts. Finally, we sealed the devices with an SU-8 epoxy protective layer that was etched to make only the central area of the nanoribbon accessible to the solution (Figure 1B).

These devices exhibited a typical FET device transfer characteristic (I_{SD}−V_g) with the source-drain current turning off at gate voltages below −1 V and rapidly increasing at the gate voltages above this value (Figure 1C). The typical field effect mobility of our SiNR FET devices was 0.014 $cm^2\ V^{-1}\ s^{-1}$ [35] and the electrical double layer capacitance per unit area was 26.4 $\mu F\ cm^{-2}$.[36]

It is also important to optimize the device sensitivity to the changes of the environment around the nanoribbon. In principle, the highest sensitivity is achieved in the subthreshold regime where device conductance depends exponentially on gate voltage.[35] However, in this regime the device conductance and, consequently, the absolute magnitude of the signal is very small. Hence, we chose to operate our devices at the gate voltage that corresponds to the maximum device transconductance (Figure 1C, dashed line), where a small change in the potential can still lead to a significant change in current/conductance.

pH sensitivity of silicon nanowire and nanoribbon-based FETs that arises from the ionization of the silanol groups on

DOI: 10.1021/acs.nanolett.8b02898
Nano Lett. 2019, 19, 629−634

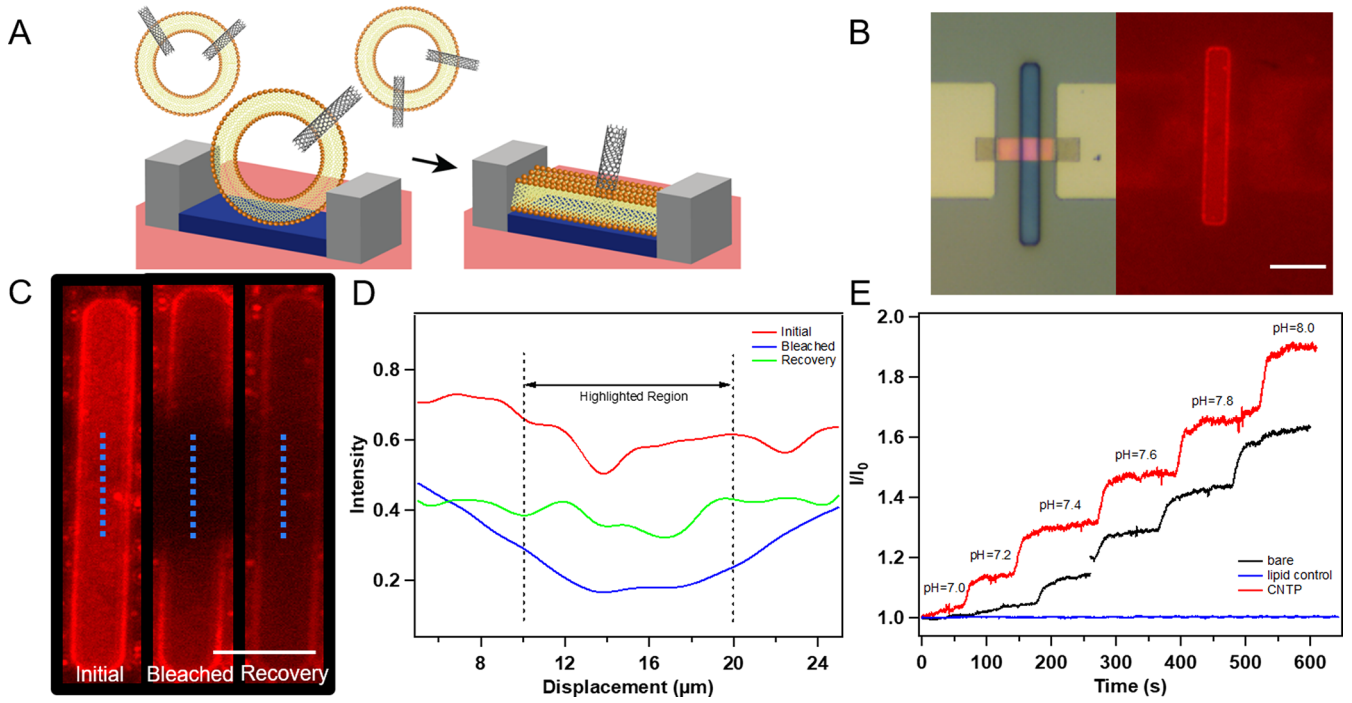

Figure 2. CNTP-SiNR pH sensors. (A) Schematics showing the vesicle fusion process used to form the lipid-CNTP coating on the devices. (B) Bright-field (left) and fluorescence microscopy images of two SiNR devices coated with lipid bilayer. Scale bar: 10 μm. (C) Fluorescence images of the etched channel region on a single device obtained before photobleaching, immediately after it, and after 20 min of recovery time. Scale bar: 10 μm. (D) Line profiles of fluorescence intensity across the Si nanoribbon (indicated by the blue dashed lines) from the images in panel C. The line profiles are low-pass filtered for clarity. (E) Time traces of the device source-drain current (I_{SD}) recorded in buffer solutions of different pH (as indicated on the graph) for the uncoated SiNR device (black), SiNR device coated with lipid bilayer (blue), and SiNR device coated with the lipid bilayer incorporating CNTP channels. All current traces were normalized to the initial current I_0.

the device surface is well documented in the literature.[37] Electrical conductance of our devices also exhibited well-defined strong response to a stepwise pH increase of the buffer solution in the fluid cell (Figure 1D). As expected, this response also did not depend on the direction or the order of the pH change. In our experimental setup, the device response kinetics are limited by the rate of buffer exchange in the fluid cell and thus do not reflect the true speed of the device.

To create the barrier lipid-CNTP membrane on the nanoribbon surface we fused DOPC−CNTP vesicles onto the device surface using protocols that we reported previously.[29] Fluorescence images (Figure 2B) indicate that Si nanoribbons were completely covered by the lipid bilayer (to assist with imaging we added a small percentage of lipid labeled with the Texas Red dye to the lipid used for vesicle preparation). To assess the bilayer quality, we conducted fluorescence recovery after photobleaching (FRAP) experiments where we used a focused light spot from the microscope to bleach a region in the lipid bilayer and then monitored the diffusion of the labeled lipid molecules back into the bleached spot (Figure 2C). Analysis of the line profiles of the resulting images shows that unbleached lipid is able to diffuse back into the bleached spot and thus confirms that the SiNR was covered with the continuous lipid bilayer.

Lipid membrane coating has a profound effect on the electrical response of the device to the pH changes (Figure 2E). The lipid coating makes the device virtually unresponsive to solution pH changes, confirming that the bilayer can act as a protective shield. Remarkably, addition of the CNTP channels, which act as high-efficiency proton conduits through the lipid bilayer, fully restores the pH sensitivity pattern of the device (Figure 2E) with the average response going back up to about 59 ± 27% per unit pH.

We also evaluated the performance of our modified pH sensors in several mixtures that contained common foulants such as bovine serum albumin (BSA), milk, or bovine blood plasma. For each of these experiments, we have characterized the ability of our sensor to respond to variations in the solution pH values before and after continuous exposure to the different foulant mixtures (average protein concentration was 1.0 mg/mL) for 60 h. Taking BSA as an example, the literature on BSA fouling contains examples of foulant concentrations that range from 20 μg/mL to 10 mg/mL and fouling times that range from 6 h to 4 days.[38−43] We designed our fouling experiments to fall roughly in the middle of those conditions range. The data showed (Figure 3) that uncoated SiNR sensors were irreversibly fouled and completely lost their pH response for all three foulants used (Figure 3A−C, blue traces). In contrast, when the lipid bilayer incorporated CNTP channels, the pH response was preserved and showed very little signs of degradation (Figure 3A−C, red traces), even in a rather complex fouling environment of blood plasma (Figure 3C). For CNTP-SiNR sensors measured in the presence of foulants, we measured pH sensitivity of 43, 64, and 35% per unit pH in BSA, milk, and bovine blood plasma, respectively.

It is possible that the lipid bilayer itself acted as an antifouling coating to prevent the protein from sticking to the device surface. To test that possibility, we have used BSA labeled with a fluorescent FITC marker and imaged the device surface after exposure to this foulant. Both uncoated and lipid−CNTP-coated devices showed significant levels of protein adsorption on the surface (Figure 3A, insets),

DOI: 10.1021/acs.nanolett.8b02898
Nano Lett. 2019, 19, 629−634

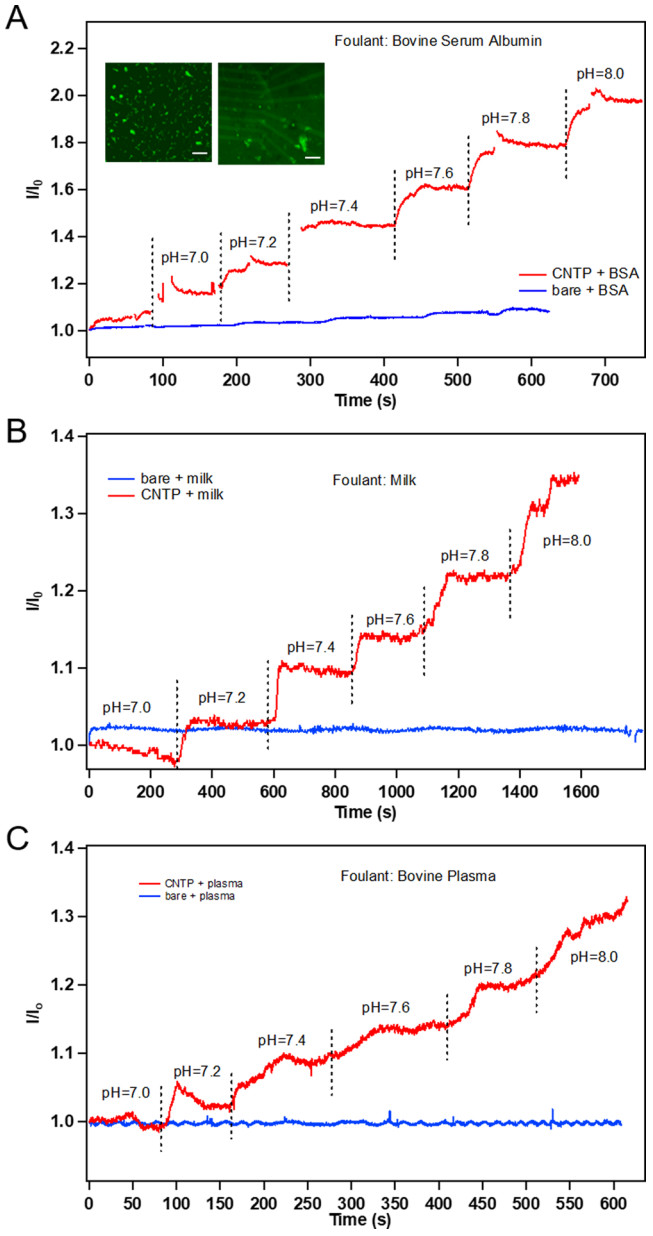

Figure 3. CNTP-SiNR sensors operation in complex fouling mixtures. (A) Time traces of a CNTP-SiNR device source-drain current (I_{SD}) recorded in buffer solutions of different pH in the presence of 1.0 mg/mL bovine serum albumin (red). Time trace of the I_{SD} for an uncoated SiNR device recorded in different pH buffers in the presence of bovine serum albumin (blue) shows strong fouling. Inset shows fluorescence microscopy images of FITC dye-labeled BSA attached to the surface of the lipid-coated (left) and uncoated (right) SiNR device chip Scale bar: 100 μm. (B) Time traces of CNTP-SiNR device (red) and uncoated SiNR device (blue) source-drain current (I_{SD}) recorded in buffer solutions of different pH after the devices were exposed for 60 h to simulated dilute milk (1.0 mg/mL milk protein in 10 mM HEPES-K, 30 mM KCl, 150 mM NaCl buffer). (C) pH response of the CNTP-SiNR device after (red) exposure for 60 h to bovine blood plasma solution (1.0 mg/mL bovine plasma in 10 mM HEPES-K, 30 mM KCl, 150 mM NaCl). A control experiment shows pH response of an uncoated SiNR device after (blue) the same 60 h exposure to bovine blood plasma. On all panels the solution pH values are indicated on the graphs.

indicating that lipid bilayer was not able to prevent protein adsorption on the device completely and that small size and high proton permeability of CNTP pores plays an important role in enabling the sensing functionality. We also note that even though our sensors show significant degree of fouling resistance they still can be defeated by a thick and dense fouling layer formed on top of the device. For example, we observed that very high concentrations of milk protein and BSA (about 40 mg/mL) that are close to the maximum solubility of the proteins tended to foul the device irreversibly even in the presence of CNTPs.

These results show that lipid coating incorporating CNTP pores can act as an effective protective membrane for Si nanoribbon devices. Moreover, proton permeability, engineered by adding CNTPs to the membrane allowed those devices to report solution pH in complex multicomponent biological fluids with high fouling propensity. CNTP robustness and tunability of their permeability characteristics also opens up opportunities to expand the performance envelope of these sensors by engineering CNTPs to transmit specific ions and small molecules while blocking other biomolecules. These capabilities could transform SiNR or a similar SiNW platform into a versatile platform-type sensing technology that could be used in applications ranging from disease diagnosis, genetic screening, and drug discovery to environmental monitoring.

Materials and Methods. *Device Fabrication.* SiNR-FET devices were fabricated from Silicon-on-Insulator (SOI) wafers (University Wafer, SIMOX, 2268). The device layer thickness was 50 nm, buried oxide (BOX) thickness was 145 nm, and the handle layer thickness was 775 μm. After careful piranha cleaning and oxygen plasma cleaning, the wafer was dehydrated and spin-coated with maN 2403 photoresist. Silicon nanoribbons (2 μm × 20 μm) were patterned with E-beam lithography (Vistec VB300 Electron Beam Lithography system) and developed in ma-D 532 Developer. After a brief descum cleaning the patterned wafer was etched at −120 °C for 20s using inductively coupled plasma (ICP) (Oxford Plasma Lab 100 Viper). Etched wafers were cleaned with acetone, rinsed with DI water, dried under nitrogen, descummed again, cleaned with acetone, rinsed with DI water, and dried under nitrogen. A thin (10 nm) dielectric silicon oxide layer on the silicon nanoribbon was then deposited using 250 cycles of plasma-enhanced atomic layer deposition at 300 °C (Oxford FlexAL). The wafers were subsequently annealed at 900 °C under nitrogen flow in a rapid thermal furnace for 10 min, followed by another acetone cleaning and DI water rinse. The wafer was dehydrated under a dry nitrogen stream and spin-coated with LOR 5A and S1805 photoresist. UV lamp was used to expose the electrode pattern. The wafer was developed in MF26A developer solution and then etched in 1:30 diluted buffer oxide etchant (BHF). The etched wafer was rinsed in DI water, dried with nitrogen and immediately transferred to the E-beam evaporator (Semicore SC600) to deposit 100 nm of nickel. Remover PG (heated to 70 °C) was used for metal liftoff. The wafer was rinsed with acetone and DI water, descummed in oxygen plasma (RIE) and then annealed in a rapid thermal annealing system at 380 °C. Finally, to create an about 0.8 μm-thick passivation layer, the device wafer was spin-coated with SU-8 (MicroChem SU-8 TF 6001) at 3k rpm and baked at 110 °C. In the final step, the small windows exposing the central regions of the nanoribbons were defined by photolithography, the wafer was baked at 110 °C, developed in SU-8 developer and descummed in oxygen plasma (RIE). Devices were diced out from the wafer and inspected with a field-emission SEM (Zeiss Gemini Ultra-55).

DOI: 10.1021/acs.nanolett.8b02898
Nano Lett. 2019, 19, 629−634

Device Performance Benchmarking. A flow cell constructed of a custom-molded polydimethylsiloxane (Sylgard 184 Silicone Elastomer, Dow Corning, 0007997641) was placed on the top surface of the device and secured to a fixture. The flow cell was connected to a syringe pump (LEGATO 110, KD Scientific, 78-8110) with LDPE micromedical tubing (Scientific Commodities Inc., BB31695-PE/3, inner diameter 0.58 mm). The flow cell also incorporated an opening for a reference Ag/AgCl microelectrode that served as a gate electrode. Transfer characteristics were typically measured with the drain-source voltage (V_{DS}) at 0.1 V. The fluid cell was filled with the 10 mM HEPES-K, 30 mM KCl, and 150 mM NaCl, buffer solution (pH = 7.2). Only the devices with threshold potentials between −0.5 and −1.5 V were used for the subsequent measurements (a higher threshold voltage typically indicated poor silicide contact between the silicon nanoribbon and nickel electrode, whereas a lower threshold voltage indicated excessive dopant levels in the SOI wafer).

Device response kinetics were measured at 100 mV source-drain voltage. To ensure high device sensitivity we chose V_G values corresponding to the steepest slope in transfer characteristics curve; for our devices, this region corresponded to −1.3 ± 0.4 V. The average pH sensitivity for the uncoated SiNR devices (defined as the percentage change in drain-source current) was 49 ± 24% per pH unit. The rate of the device response does not reflect the intrinsic speed of the device; rather, SiNR device response is limited by the kinetics of the buffer exchange in the fluid cell, which was limited by the maximum syringe pump flow rate of 0.4 mL/min (higher flow rates tended to infuse air bubbles into the chamber and caused noisy spikes in the current readout).

Lipid Membrane Coating. CNTPs, DOPC LUVs, and CNTP-LUVs were prepared using previously reported protocols.[44] The lipid membrane coating was formed using Ca^{2+} induced vesicle fusion. Briefly, the fluid cell was filled with the solution of LUVs in 10 mM HEPES-K, 30 mM KCl and 150 mM NaCl buffer solution, incubated for 20 min, then washed with 50 mM $CaCl_2$ and 10 mM HEPES buffer, incubated for 10 min, and flushed with 10 mM HEPES-K, 30 mM KCl, and 150 mM NaCl buffer solution to get the lipid bilayer membrane on the device surface. Fluorescence microscopy images of the device surface were taken with Leica DM4000 equipped with Hamamatsu Orca Flash 4.0 camera. For the fluorescence recovery after photobleaching (FRAP) measurements after taking the initial image, a spot was bleached in the center of the device for 10 min. The recovery image was taken after 20 min of recovery.

Antifouling Tests. Bovine serum albumin (BSA, Sigma, SLBK3715 V) was used at a concentration of 1.0 mg/mL in 10 mM HEPES-K, 30 mM KCl, and 150 mM NaCl buffer. Milk solution was prepared from condensed milk powder (purchased from a Target store) dissolved in 10 mM HEPES-K, 30 mM KCl, and 150 mM NaCl buffer to achieve a final concentration of 1.0 mg/mL milk protein density. Bovine plasma (Sigma, SLBS4463) was diluted in 10 mM HEPES-K, 30 mM KCl, and 150 mM NaCl buffer to a final concentration of 1.0 mg/mL. In a typical fouling experiment, the foulant solution was introduced into the fluid cell and the whole device assembly was kept in a humid environment for 60 h with aluminum foil wrapped on the outside to avoid light exposure. To retest the same device performance without lipid/CNTP coating it was removed by surfactant (Triton X-100, VWR, 0606C284) and the same fouling experiment protocol was repeated.

AUTHOR INFORMATION

Corresponding Author

*E-mail: noy1@llnl.gov.

ORCID

Huanan Zhang: 0000-0002-3437-2510

Aleksandr Noy: 0000-0003-4924-2652

Present Addresses

§(H.Z.) Department of Chemical Engineering, University of Utah, Salt Lake City, UT 84112.

‖(R.H.T.) PACT Pharma, Hayward, CA 94545.

Notes

The authors declare no competing financial interest.

ACKNOWLEDGMENTS

X.C. acknowledges the fellowship support from UC Office of the President, UC Laboratory Fees Research Program under Grant LGF-18-545710. This work was supported by the U.S. Department of Energy, Office of Basic Energy Sciences, Division of Materials Sciences and Engineering. Work at LLNL was performed under the auspices of the U.S. Department of Energy under contract DE-AC52-07NA27344. Work at the Molecular Foundry at LBL was supported by the Office of Science, Office of Basic Energy Sciences, of the U.S. Department of Energy under contract DE-AC02-05CH11231.

REFERENCES

(1) Alberts, B.; Bray, D.; Lewis, J.; Raff, M.; Roberts, K.; Watson, J. D. *Mol. Biol. Cell*, 5th ed.; Garland Science: New York, 2007; p 1728.

(2) Damaghi, M.; Wojtkowiak, J. W.; Gillies, R. J. *Front. Physiol.* **2013**, *4*, 370.

(3) Pavlov, I.; Kaila, K.; Kullmann, D. M.; Miles, R. *J. Physiol.* **2013**, *591*, 765−74.

(4) Ronkainen, N. J.; Halsall, H. B.; Heineman, W. R. *Chem. Soc. Rev.* **2010**, *39* (5), 1747−1763.

(5) Lin, P.; Yan, F.; Chan, H. L. *ACS Appl. Mater. Interfaces* **2010**, *2* (6), 1637−1641.

(6) Chen, K.-I.; Li, B.-R.; Chen, Y.-T. *Nano Today* **2011**, *6* (2), 131−154.

(7) Zheng, G.; Patolsky, F.; Cui, Y.; Wang, W. U.; Lieber, C. M. *Nat. Biotechnol.* **2005**, *23* (10), 1294−1301.

(8) Lin, T.-W.; Hsieh, P.-J.; Lin, C.-L.; Fang, Y.-Y.; Yang, J.-X.; Tsai, C.-C.; Chiang, P.-L.; Pan, C.-Y.; Chen, Y.-T. *Proc. Natl. Acad. Sci. U. S. A.* **2010**, *107* (3), 1047−1052.

(9) Wang, W. U.; Chen, C.; Lin, K.-h.; Fang, Y.; Lieber, C. M. *Proc. Natl. Acad. Sci. U. S. A.* **2005**, *102* (9), 3208−3212.

(10) Chua, J. H.; Chee, R.-E.; Agarwal, A.; Wong, S. M.; Zhang, G.-J. *Anal. Chem.* **2009**, *81* (15), 6266−6271.

(11) Stern, E.; Klemic, J.; Routenberg, D.; Wyrembak, P.; Turner-Evans, D.; Hamilton, A.; LaVan, D.; Fahmy, T.; Reed, M. *Nature* **2007**, *445* (7127), 519−522.

(12) Stern, E.; Vacic, A.; Rajan, N.; Criscione, J.; Park, J.; Ilic, B.; Mooney, D.; Reed, M.; Fahmy, T. *Nat. Nanotechnol.* **2010**, *5* (2), 138−142.

(13) Hahm, J.-i.; Lieber, C. M. *Nano Lett.* **2004**, *4* (1), 51−54.

(14) Li, Z.; Chen, Y.; Li, X.; Kamins, T.; Nauka, K.; Williams, R. S. *Nano Lett.* **2004**, *4* (2), 245−247.

(15) Ganguly, A.; Chen, C.-P.; Lai, Y.-T.; Kuo, C.-C.; Hsu, C.-W.; Chen, K.-H.; Chen, L.-C. *J. Mater. Chem.* **2009**, *19* (7), 928−933.

(16) Patolsky, F.; Zheng, G. F.; Hayden, O.; Lakadamyali, M.; Zhuang, X. W.; Lieber, C. M. *Proc. Natl. Acad. Sci. U. S. A.* **2004**, *101* (39), 14017−14022.

DOI: 10.1021/acs.nanolett.8b02898
Nano Lett. 2019, 19, 629−634

(17) Banerjee, I.; Pangule, R. C.; Kane, R. S. *Adv. Mater.* **2011**, *23* (6), 690−718.
(18) Krishnan, S.; Weinman, C. J.; Ober, C. K. *J. Mater. Chem.* **2008**, *18* (29), 3405−3413.
(19) Vaisocherová, H.; Brynda, E.; Homola, J. *Anal. Bioanal. Chem.* **2015**, *407* (14), 3927−3953.
(20) Zhang, P.; Lin, L.; Zang, D.; Guo, X.; Liu, M. *Small* **2017**, *13* (4), 1503334.
(21) Nir, S.; Reches, M. *Curr. Opin. Biotechnol.* **2016**, *39*, 48−55.
(22) Detty, M. R.; Ciriminna, R.; Bright, F. V.; Pagliaro, M. *Acc. Chem. Res.* **2014**, *47* (2), 678−687.
(23) White, S. P.; Sreevatsan, S.; Frisbie, C. D.; Dorfman, K. D. *ACS Sens.* **2016**, *1* (10), 1213−1216.
(24) Meyburg, S.; Goryll, M.; Moers, J.; Ingebrandt, S.; Böcker-Meffert, S.; Lüth, H.; Offenhäusser, A. *Biosens. Bioelectron.* **2006**, *21* (7), 1037−1044.
(25) Meyburg, S.; Stockmann, R.; Moers, J.; Offenhäusser, A.; Ingebrandt, S. *Sens. Actuators, B* **2007**, *128* (1), 208−217.
(26) Wu, T.; Alharbi, A.; You, K.-D.; Kisslinger, K.; Stach, E. A.; Shahrjerdi, D. *ACS Nano* **2017**, *11* (7), 7142−7147.
(27) Ahn, J.-H.; Choi, S.-J.; Han, J.-W.; Park, T. J.; Lee, S. Y.; Choi, Y.-K. *Nano Lett.* **2010**, *10* (8), 2934−2938.
(28) Artyukhin, A. B.; Shestakov, A. I.; Harper, J.; Bakajin, O.; Stroeve, P.; Noy, A. *J. Am. Chem. Soc.* **2005**, *127* (20), 7538−7542.
(29) Misra, N.; Martinez, J. A.; Huang, S.-C.; Wang, Y.; Stroeve, P.; Grigoropoulos, C.; Noy, A. *Proc. Natl. Acad. Sci. U. S. A.* **2009**, *106* (33), 13780−13784.
(30) Huang, S.-C.; Artyukhin, A.; Misra, N.; Martinez, J.; Stroeve, P.; Grigoropoulos, C.; Ju, J.-W.; Noy, A. *Nano Lett.* **2010**, *10* (5), 1812−1816.
(31) Geng, J.; Kim, K.; Zhang, J.; Tunuguntla, R.; Comolli, L.; Allen, F.; Cho, K.; Munoz, D.; Wang, Y.; Grigoropoulos, C. P.; Ajo-Franklin, C. M.; Noy, A. *Nature* **2014**, *514*, 612−615.
(32) Tunuguntla, R.; Allen, F.; Kim, K.; Bellivieau, A.; Noy, A. *Nat. Nanotechnol.* **2016**, *11*, 639−644.
(33) Wang, M. C. P.; Gates, B. D. *Mater. Today* **2009**, *12* (5), 34−43.
(34) Su, B.; Wu, Y.; Jiang, L. *Chem. Soc. Rev.* **2012**, *41* (23), 7832−7856.
(35) Sze, S. M.; Ng, K. K. *Physics of semiconductor devices*; John Wiley & Sons, 2006.
(36) Park, S.; Lee, S.; Kim, C.-H.; Lee, I.; Lee, W.-J.; Kim, S.; Lee, B.-G.; Jang, J.-H.; Yoon, M.-H. *Sci. Rep.* **2015**, *5*, 13088.
(37) Mu, L.; Chang, Y.; Sawtelle, S. D.; Wipf, M.; Duan, X.; Reed, M. A. *IEEE Access* **2015**, *3*, 287−302.
(38) Wang, Y.-N.; Tang, C. Y. *J. Membr. Sci.* **2011**, *376* (1), 275−282.
(39) Li, Q.; Xu, Z.; Pinnau, I. *J. Membr. Sci.* **2007**, *290* (1−2), 173−181.
(40) Park, J.-S.; Chilcott, T.; Coster, H.; Moon, S.-H. *J. Membr. Sci.* **2005**, *246* (2), 137−144.
(41) Park, J.-S.; Choi, J.-H.; Yeon, K.-H.; Moon, S.-H. *J. Colloid Interface Sci.* **2006**, *294* (1), 129−138.
(42) Mo, H.; Tay, K. G.; Ng, H. Y. *J. Membr. Sci.* **2008**, *315* (1), 28−35.
(43) Meng, H.; Cheng, Q.; Wang, H.; Li, C. *J. Chem.* **2014**, *2014*, 9.
(44) Tunuguntla, R. H.; Frolov, V.; Noy, A.; et al. *Nat. Protoc.* **2016**, *11* (10), 2029−2047.

DOI: 10.1021/acs.nanolett.8b02898
Nano Lett. 2019, 19, 629−634